

Qun Wei*, Meiguang Zhang*, Haiyan Yan, Renxian Li, Xuanmin Zhu, Zhengzhe Lin and Ronghui Yao

A New Superhard Phase of C_3N_2 Polymorphs

DOI 10.1515/zna-2015-0270

Received June 16, 2015; accepted October 6, 2015

Abstract: Carbon nitrides are excellent candidates for extreme hardness materials. In this work, a new $I\bar{4}3m$ phase of C_3N_2 has been uncovered by replacing part of the nitrogen atoms in the cage-like diamondoid nitrogen N_{10} with carbon atoms. This phase is mechanically and dynamically stable up to at least 50 GPa. The elastic anisotropy of $I\bar{4}3m$ - C_3N_2 is investigated by comparing with previously proposed α - C_3N_2 . The tensile directional dependence of Young's modulus obeys the following trend: $E_{[111]} > E_{[110]} > E_{[100]}$. Electronic structure calculations reveal that $I\bar{4}3m$ - C_3N_2 is hole conducting. Hardness calculation shows that the $I\bar{4}3m$ - C_3N_2 is superhard with a hardness of 72.9 GPa.

Keywords: Crystal Structure; Elastic Properties; Electronic Structure; First Principles Calculations.

1 Introduction

Searching new superhard material has been concentrated by researchers in recent years. Usually, borides, nitrides, and covalent of light elements (Be, B, C, N, etc.) are regarded as candidates of superhard materials [1–5]. Among these materials, carbon nitrides are a typical group. Theoretically, some superhard phases of carbon nitrides are predicted by first principles calculations before experimental preparation. Liu and Cohen [6, 7] presented a hexagonal superhard β - C_3N_4 structure, which has been obtained experimentally later [8, 9]. Then, C_3N_4 and $C_{11}N_4$ are theoretically proved to be superhard materials

[10]. The theoretical hardness of C_3N_4 is 85.7 GPa [11], which is close to that of diamond. In addition, a group of tetragonal crystalline carbon mononitrides (CN) have been predicted [12]. By replacing part of the nitrogen atoms in the cubic gauche of nitrogen, a new superhard CN phase (cg-CN) has been proposed [13]. It is interesting that the cg-CN is found to be a metallic compound, although most superhard carbon nitrides are insulators or semiconductors. For example, Wehrich et al. proposed a $Pa\bar{3}$ phase CN_2 with a large bulk modulus of 405 GPa [14]. Using crystal structure prediction technique, a body-centered tetragonal CN_2 has been uncovered [15]. The ideal strength and hardness calculation show that bct- CN_2 is superhard with the hardness of 77.4 GPa. Tian et al. proposed $Pm\bar{3}m$ phase C_3N_2 (α - C_3N_2) at pressure below 1.0 GPa and $P\bar{4}3m$ phase (β - C_3N_2) at high pressure [16]. The Vickers hardness of both phases are approximately 86 GPa.

In the present work, we present a new metastable C_3N_2 phase by replacing part of the nitrogen atoms in the cage-like diamondoid nitrogen N_{10} [17] with carbon atoms. In N_{10} crystal, there are two inequivalent sites 12e and 8c. We replaced the N atoms in the Wyckoff position 12e (C_3N_2) and 8c (C_2N_3) with carbon atoms, respectively. Both C_3N_2 and C_2N_3 have the same space group $I\bar{4}3m$. Phonon spectra calculations show that C_2N_3 is not stable, whereas C_3N_2 is found to be mechanically and dynamically stable up to at least 50 GPa, with a high hardness of 72.9 GPa.

2 Computational Details

Our calculations are performed using the VASP code [18] with the generalised gradient approximation (GGA) [19] and local density approximation (LDA) [20] for exchange correlation functional. The integration in the Brillouin zone is employed using the Monkhorst–Pack scheme ($11 \times 11 \times 11$), and the energy cut-off of 900 eV was chosen to ensure that energy calculations are converged to better than 1 meV/atom. The electron–core interactions are included by using the frozen-core all-electron projector augmented wave (PAW) method [21], with C: $2s^2 2p^2$ and N: $2s^2 2p^3$ treated as the valence electrons. The elastic constants are determined from evaluation of stress tensor-generated small strain. Bulk modulus, shear modulus,

*Corresponding authors: Qun Wei, School of Physics and Optoelectronic Engineering, Xidian University, Xi'an 710071, PR China, E-mail: weiaqun@163.com; and Meiguang Zhang, Department of Physics and Information Technology, Baoji University of Arts and Sciences, Baoji 721016, PR China, E-mail: zhmgbj@126.com
 Haiyan Yan: Department of Chemistry and Chemical Engineering, Baoji University of Arts and Sciences, Baoji 721013, PR China
 Renxian Li, Xuanmin Zhu, Zhengzhe Lin and Ronghui Yao: School of Physics and Optoelectronic Engineering, Xidian University, Xi'an 710071, PR China

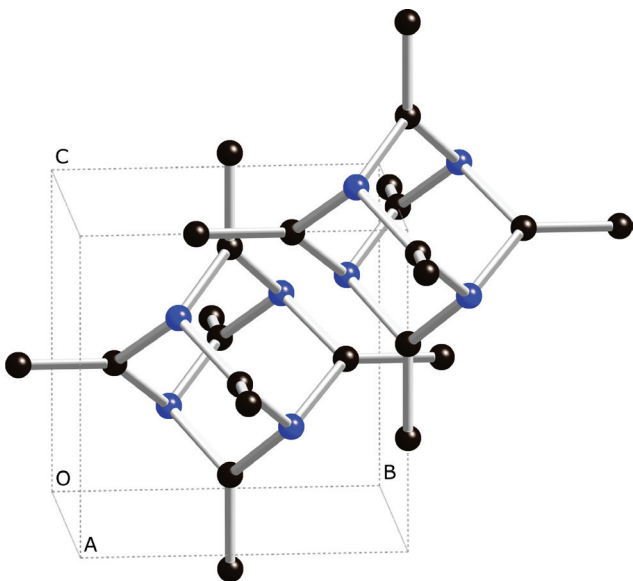
Table 1: Equilibrium lattice parameters (in Å), Wyckoff positions, volume of unit cell (in Å³), bonding length (in Å), EOS-fitted bulk modulus (in GPa) and its derivative for $I\bar{4}3m-C_3N_2$.

Crystal	Method	a_0	Wyckoff positions	V_0	d_{C-N}	d_{C-C}	B_0	B'_0
$I\bar{4}3m-C_3N_2$	GGA	4.9202	C(0.0, 0.0, 0.3537) N(0.8281, 0.8281, 0.8281)	119.1	1.4936	1.4394	358	3.78
	LDA	4.8549	C(0.0, 0.0, 0.3534) N(0.8281, 0.8281, 0.8281)	114.4	1.4729	1.4236	398	3.71
$\alpha-C_3N_2$	GGA	5.092		132.0	1.4351	1.5886	373	3.78
$\beta-C_3N_2$	GGA	5.088		131.7	1.4314	1.5874	328	2.98
					1.4405			

Young's modulus, and Poisson's ratio are estimated by using Voigt–Reuss–Hill approximation [22].

3 Results and Discussions

After relaxing the crystal structure at 0 GPa, we obtain that this structure has a lattice parameter of 4.9202 Å within GGA. The optimised parameters for C_3N_2 at 0 GPa within GGA and LDA are listed in Table 1, and the unit cell structure is shown in Figure 1. In this structure, there are two inequivalent C6N4 cages. One is at body centered site, and the other is at the vertex site. Each cage connects with six equivalent cages by C–C bonds, whereas there is no covalent bonding between center and vertex cages. The C6N4 cage is formed by 12 C–N bonds, and the bond angles of C–N–C and N–C–N are 110.0 and 106.4 degree, respectively. The P–V relations of $\alpha-C_3N_2$, $\beta-C_3N_2$,

**Figure 1:** Crystal structure of $I\bar{4}3m-C_3N_2$. The N atoms are represented in blue and C atoms black.

and $I\bar{4}3m-C_3N_2$ are plotted in Figure 2, as well as those of c-BN and diamond. We can see that the incompressibility of $I\bar{4}3m-C_3N_2$ is larger than $\beta-C_3N_2$ and almost the same as $\alpha-C_3N_2$ and c-BN. We can deduce that the bulk modulus of these three phases of C_3N_2 should follow the same order. To verify this, we obtain the values of equilibrium bulk modulus and its pressure derivative by fitting the E–V data at different pressure into the third-order Birch–Murnaghan equation of state (EOS) [23], and the results are listed in Table 1. The fitted bulk modulus for $I\bar{4}3m-C_3N_2$ is 358 GPa within GGA, which is larger than that of $\beta-C_3N_2$ (328 GPa) and slightly less than that of $\alpha-C_3N_2$ (373 GPa).

In order to check the stability of $I\bar{4}3m-C_3N_2$, we calculate the elastic constants (see Tab. 2) and phonon frequencies (Fig. 3). For cubic crystal, the mechanical stability criteria at 0 GPa are as follows [24]: $C_{11} + 2C_{12} > 0$, $C_{44} > 0$, and $C_{11} - C_{12} > 0$. When a hydrostatic pressure is applied on crystals, the mechanical stability criteria for cubic crystals are as follows [25]: $C_{11} + 2C_{12} + P > 0$, $C_{44} - P > 0$, and $C_{11} - C_{12} - 2P > 0$. One can see from Table 2 that the

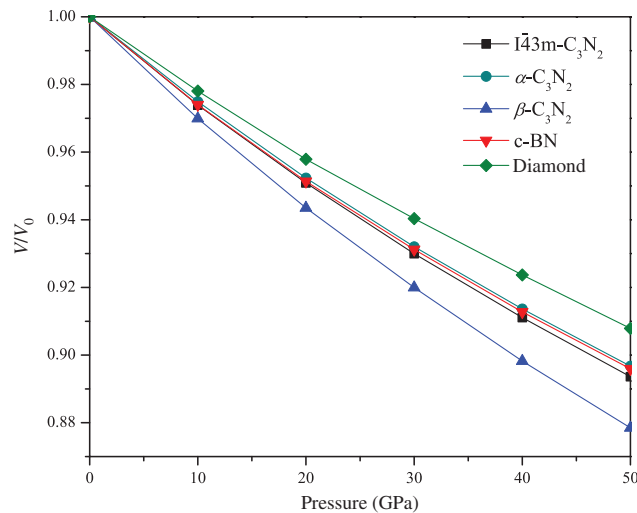
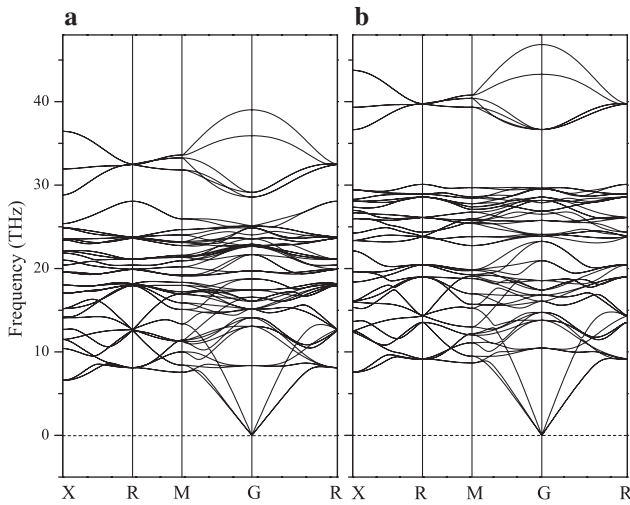
**Figure 2:** Variation of ratio V/V_0 with pressures for $I\bar{4}3m-C_3N_2$, $\alpha-C_3N_2$, $\beta-C_3N_2$, c-BN, and diamond.

Table 2: Calculated elastic constants C_{ij} , bulk modulus B , shear modulus G , Young's modulus E , and hardness H_k (in unit of GPa) of $\bar{I}43m-C_3N_2$.

Crystal	Method	C_{11}	C_{12}	C_{44}	B	G	E	ν	G/B	H_k
$\bar{I}43m-C_3N_2$	GGA	653	214	240	361	232	572	0.2355	0.64	72.9
	LDA	698	251	254	400	241	604	0.2487	0.60	76.8
$\alpha-C_3N_2$	GGA	856	134	320	374	335	775	0.155	0.90	65.1
	GGA [16]	876	137	327	380	365	829	0.136	0.96	
$\beta-C_3N_2$	GGA	850	135	321	373	335	774	0.154	0.90	65.3
	GGA [16]	834	98	329	343	368	813	0.105	1.07	

Also shown are Poisson's ratio ν and G/B ratio.

**Figure 3:** Phonon dispersion curve of $\bar{I}43m-C_3N_2$ at 0 GPa (a) and 50 GPa (b).

calculated elastic constants are satisfied above mechanical stability criteria, which shows the mechanical stability of $\bar{I}43m-C_3N_2$ up to 50 GPa. The phonon dispersion curves for $\bar{I}43m-C_3N_2$ at 0 and 50 GPa are shown in Figure 3. No imaginary phonon frequency is observed in the whole Brillouin zone, indicating its dynamical stability in the range from 0 to at least 50 GPa. In the pressure range, we studied that the enthalpy of $\bar{I}43m-C_3N_2$ is always higher than that of $\alpha-C_3N_2$ or $\beta-C_3N_2$, so it is a metastable phase of C_3N_2 . The calculated bulk modulus (see Tab. 2) by means of the Voigh–Reuss–Hill approximation method is consistent with the EOS fitting results. The shear modulus quantifies its resistance to shear deformation and is a better indicator of potential hardness for ionic and covalent materials [26]. Young's modulus E is defined as the ratio between stress and strain and is used to provide a measure of the stiffness of the solid. Compared to $\alpha-C_3N_2$ and $\beta-C_3N_2$, the less E of $\bar{I}43m-C_3N_2$ means that $\alpha-C_3N_2$ and $\beta-C_3N_2$ are stiffer than $\bar{I}43m-C_3N_2$. The G/B ratio can be used to determine the relative directionality of the bonding in the material. The calculated ratio G/B for $\bar{I}43m-C_3N_2$ is 0.64, which is

smaller than that of $\alpha-C_3N_2$ and $\beta-C_3N_2$ at the GGA level. This shows that the directionality of C–N bond in $\bar{I}43m-C_3N_2$ is weaker than that of $\alpha-C_3N_2$ and $\beta-C_3N_2$.

Elastic anisotropy can give a prediction of the arrangement of the atoms in each direction, the bonding properties, and some chemical characters in different directions of materials. To illustrate the elastic anisotropy in detail, it is worthy to study the variation of Young's modulus and shear modulus with direction. The variation of Young's modulus along an arbitrary $[hkl]$ direction for orthorhombic symmetry can be written as

$$E^{-1} = s_{11}(\alpha^4 + \beta^4 + \gamma^4) + (2s_{12} + s_{44})(\alpha^2\beta^2 + \beta^2\gamma^2 + \alpha^2\gamma^2) \quad (1)$$

where α , β , and γ are the direction cosines of the tensile stress direction, and s_{11} , s_{12} , and s_{44} are elastic compliance constants. The relations between s_{ij} and C_{ij} are $s_{11} = (C_{11} + C_{12}) / (C_{11}^2 + C_{11}C_{12} - 2C_{12}^2)$, $s_{12} = -C_{12} / (C_{11}^2 + C_{11}C_{12} - 2C_{12}^2)$, and $s_{44} = 1/C_{44}$. The directional dependence of Young's modulus for $\bar{I}43m-C_3N_2$ is shown in Figure 4. $\beta-C_3N_2$ has almost the same elastic constants as $\alpha-C_3N_2$ (see Tab. 2); thus, they should have the same anisotropy properties. So, we only illustrate the directional dependence of Young's modulus for $\alpha-C_3N_2$ in Figure 4 for comparison. It can be seen that the nonspherical nature of $\bar{I}43m-C_3N_2$ and $\alpha-C_3N_2$ in Figure 4a and b shows the clear anisotropy of Young's modulus. The maximum and minimum of Young's modulus of $\bar{I}43m-C_3N_2$ in all directions are 589 and 547 GPa, respectively. The ratio $E_{\max}/E_{\min} = 1.08$ is slightly less than that of $\alpha-C_3N_2$ ($E_{\max}/E_{\min} = 820/747 = 1.10$). The mean value of $\bar{I}43m-C_3N_2$ in all directions is 568 GPa, which matches well with the value calculated by the Voigt–Reuss–Hill approximation (572 GPa, see Tab. 2). In order to get a better understanding of the origin of the changes in Young's modulus along different directions, the orientation dependences of Young's modulus for $\bar{I}43m-C_3N_2$ and $\alpha-C_3N_2$ are calculated when the tensile axis is within specific planes, as shown in Figure 5. From (1), we can obtain $E^{-1} = s_{11} + \sin^2\theta(2s_{12} + s_{44} - 2s_{11})/4$ for Young's modulus in (100) plane, where θ is the angle between

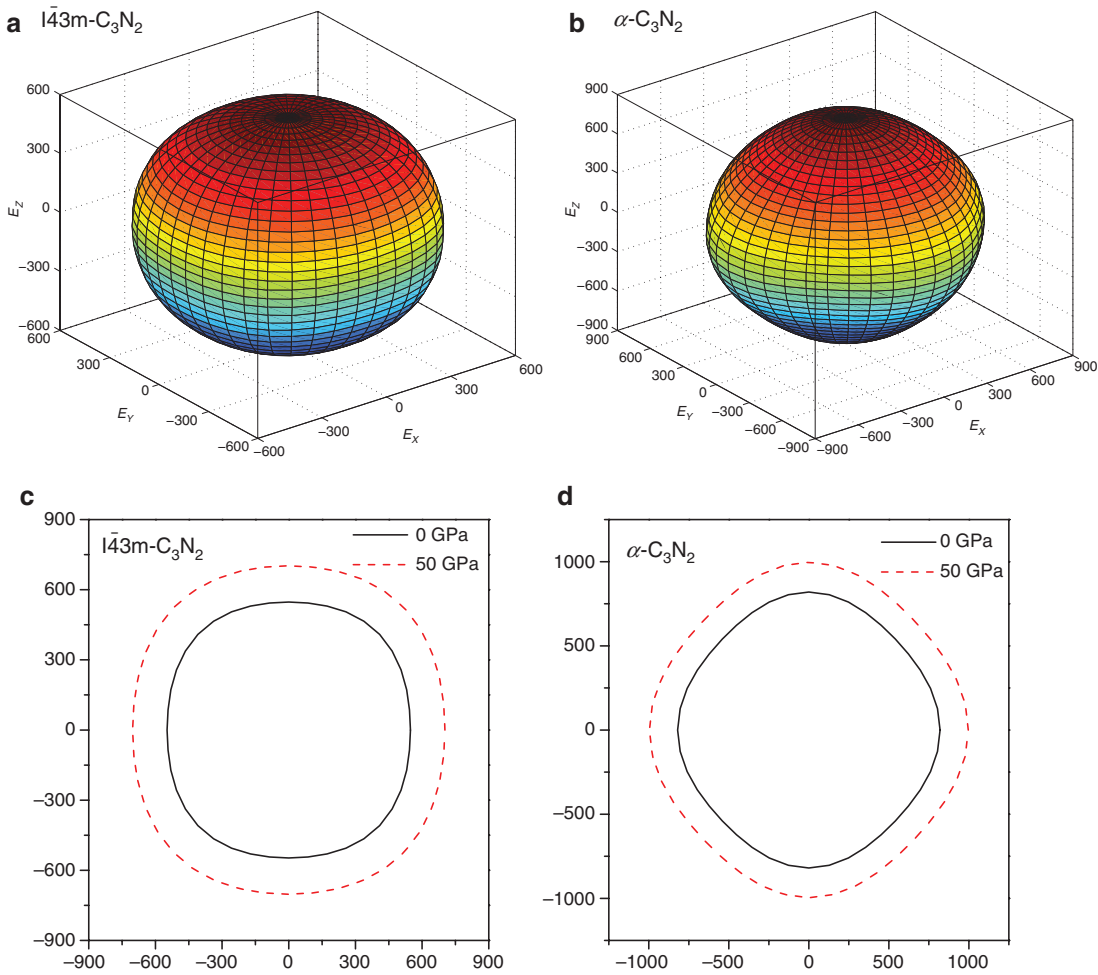


Figure 4: Illustrations of directional dependence of Young's modulus for $I\bar{4}3m-C_3N_2$ (a) and $\alpha-C_3N_2$ (b), and projections in xy plane of directional dependent Young's modulus for $I\bar{4}3m-C_3N_2$ (c) and $\alpha-C_3N_2$ (d) at 0 and 50 GPa.

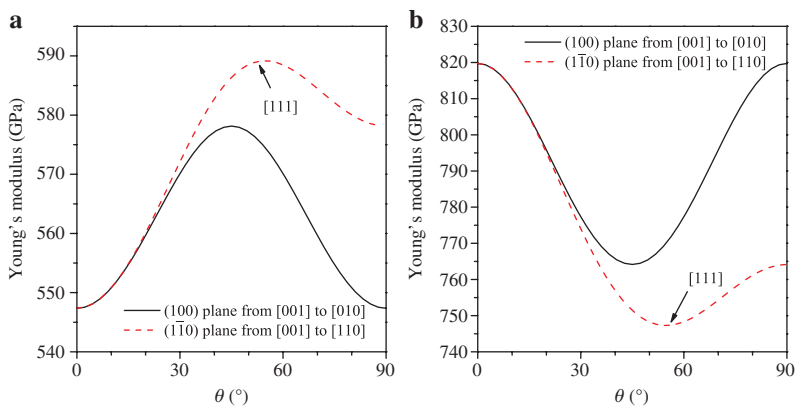


Figure 5: Plots of Young's modulus for different crystallographic directions for $I\bar{4}3m-C_3N_2$ (a) and $\alpha-C_3N_2$ (b).

tensile stress and [001], and $E^{-1} = \sin^4\theta(2s_{11} + 2s_{12} + s_{44})/4 + s_{11}\cos^4\theta + \sin^22\theta(2s_{12} + s_{44})/4$ for Young's modulus in (110) plane, where θ is the angle between tensile stress and [001]. The maximum of Young's modulus of $I\bar{4}3m-C_3N_2$ is along [111] direction, whereas the minimum is along

[100]. The order of Young's modulus as a function of the principal crystal tensile for $I\bar{4}3m-C_3N_2$ is $E_{[111]} > E_{[110]} > E_{[100]}$. For $\alpha-C_3N_2$, the ordering is $E_{[100]} > E_{[110]} > E_{[111]}$. Using the Lyakhov-Oganov model [27], the hardness of $I\bar{4}3m-C_3N_2$, as well as the hardness of $\alpha-C_3N_2$ and $\beta-C_3N_2$, is calculated

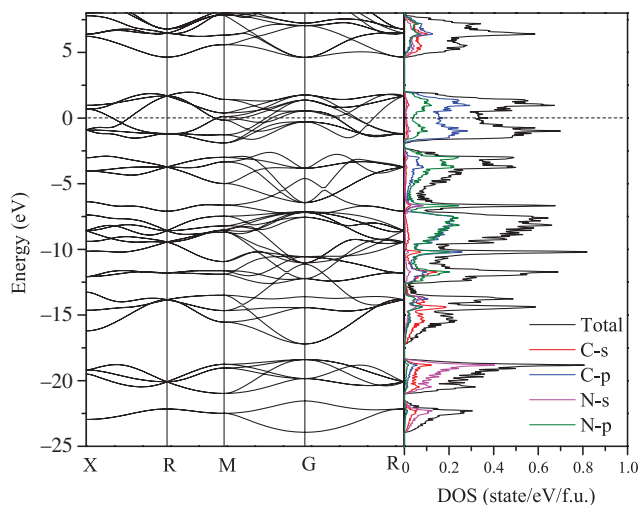


Figure 6: Band structure and DOS for $I\bar{4}3m-C_3N_2$.

and listed in Table 2. The hardness of $I\bar{4}3m-C_3N_2$ is 72.9 GPa within GGA. This shows that $I\bar{4}3m-C_3N_2$ is a superhard material. Since C–C bond is a strong covalent bond, the shorter C–C bonds usually correspond to harder materials. For $I\bar{4}3m-C_3N_2$, the C–C bond length is shorter than that of $\alpha-C_3N_2$ and $\beta-C_3N_2$, so the hardness of $I\bar{4}3m-C_3N_2$ is larger than that of $\alpha-C_3N_2$ and $\beta-C_3N_2$.

To obtain a deeper insight into the hardness of the $I\bar{4}3m-C_3N_2$, we calculate the band structure and density of state (DOS) and the atom resolved partial density of state (PDOS) of $I\bar{4}3m-C_3N_2$ at 0 GPa, as shown in Figure 6. It is found that $I\bar{4}3m-C_3N_2$ is metallic due to the finite electronic DOS at the Fermi level. The gap above Fermi level shows that $I\bar{4}3m-C_3N_2$ is a hole conductor, similar to BC_5 [28] and BC_7 [29]. From inspection of PDOS curves, it can be seen that C-p orbitals have a significant hybridisation with N-p orbitals near the Fermi level, signifying the strong C–N covalent bonding nature.

4 Conclusions

A new $I\bar{4}3m-C_3N_2$ phase has been uncovered by replacing nitrogen atoms of N_{10} with carbon atoms. Elastic and phonon calculations show that this phase is mechanically and dynamically stable up to at least 50 GPa. We have investigated the structural, mechanical, and electronic properties of $I\bar{4}3m-C_3N_2$ using first principles calculations. The tensile directional dependence of Young's modulus obeys the following trend: $E_{[111]} > E_{[110]} > E_{[100]}$. The calculated results demonstrate that $I\bar{4}3m-C_3N_2$ has large bulk and shear moduli. The hardness of 72.9 GPa illustrates its superhard character.

Acknowledgments: This work was supported by the Fundamental Research Funds for the Central Universities, the National Natural Science Foundation of China (Grant No. 11204007), the Natural Science Basic Research plan in Shaanxi Province of China (Grant Nos 2012JQ1005 and 2013JQ1007), and Education Committee Natural Science Foundation in Shaanxi Province of China (Grant No. 2013JK0638).

References

- [1] Y. Tian, B. Xu, D. Yu, Y. Ma, Y. Wang, et al., *Nature* **493**, 385 (2013).
- [2] M. Zhang, Q. Wei, H. Yan, Y. Zhao, and H. Wang, *J. Phys. Chem. C* **118**, 3202 (2014).
- [3] X. Wang, *J. Chem. Phys.* **137**, 184506 (2012).
- [4] Q. Wei, M. Zhang, L. Guo, H. Yan, X. Zhu, et al., *Chem. Phys.* **415**, 36 (2013).
- [5] H. Yan, M. Zhang, Q. Wei, and P. Guo, *Comput. Mater. Sci.* **68**, 174 (2013).
- [6] A. Liu and M. Cohen, *Science* **245**, 841 (1989).
- [7] A. Liu and M. Cohen, *Phys. Rev. B* **41**, 10727 (1990).
- [8] K. Yu, M. Cohen, E. Haller, W. Hansen, A. Liu, et al., *Phys. Rev. B* **49**, 5034 (1994).
- [9] C. Niu, Y. Z. Lu, and C. M. Lieber, *Science* **261**, 334 (1993).
- [10] M. Mattesini and S. Matar, *Phys. Rev. B* **65**, 075110 (2002).
- [11] Y. Zhang, H. Sun, and C. Chen, *Phys. Rev. B* **76**, 144101 (2007).
- [12] E. Kim, C. Chen, T. Köhler, M. Elstner, and T. Frauenheim, *Phys. Rev. Lett.* **86**, 652 (2001).
- [13] X. Wang, K. Bao, F. Tian, X. Meng, C. Chen, et al., *J. Chem. Phys.* **133**, 044512 (2010).
- [14] R. Wehrich, V. Eyert, and S. F. Matar, *Chem. Phys. Lett.* **373**, 636 (2003).
- [15] Q. Li, H. Liu, D. Zhou, W. Zheng, Z. Wu, et al., *Phys. Chem. Chem. Phys.* **14**, 13081 (2012).
- [16] F. Tian, J. Wang, Z. He, Y. Ma, L. Wang, et al., *Phys. Rev. B* **78**, 235431 (2008).
- [17] X. Wang, Y. Wang, M. Miao, X. Zhong, J. Lv, et al., *Phys. Rev. Lett.* **109**, 175502 (2012).
- [18] G. Kresse and J. Furthmüller, *Phys. Rev. B* **54**, 11169 (1996).
- [19] J. P. Perdew, K. Burke, and M. Ernzerhof, *Phys. Rev. Lett.* **77**, 3865 (1996).
- [20] D. M. Ceperley and B. J. Alder, *Phys. Rev. Lett.* **45**, 566 (1980).
- [21] G. Kresse and D. Joubert, *Phys. Rev. B* **59**, 1758 (1999).
- [22] R. Hill, *Proc. Phys. Soc. London* **65**, 349 (1952).
- [23] F. Birch, *Phys. Rev.* **71**, 809 (1947).
- [24] Z. Wu, E. Zhao, H. Xiang, X. Hao, X. Liu, et al., *Phys. Rev. B* **76**, 054115 (2007).
- [25] J. Wang, J. Li, S. Yip, S. Phillpot, and D. Wolf, *Phys. Rev. B* **52**, 12627 (1995).
- [26] J. M. Léger, P. Djemia, F. Ganot, J. Haines, A. S. Pereira, et al., *Appl. Phys. Lett.* **79**, 2169 (2001).
- [27] A. Lyakhov and A. Oganov, *Phys. Rev. B* **84**, 092103 (2011).
- [28] Q. Li, H. Wang, Y. Tian, Y. Xia, T. Cui, et al., *J. Appl. Phys.* **108**, 023507 (2010).
- [29] H. Liu, Q. Li, L. Zhu, and Y. Ma, *Solid State Commun.* **151**, 716 (2011).